ACS Macro Letters

pubs.acs.org/macroletters Letter

Polymer Chains Fold Prior to Crystallization

Fan Jin,[#] Shichen Yuan,[#] Shijun Wang, Yi Zhang, Ying Zheng, You-lee Hong, and Toshikazu Miyoshi*

Cite This: *ACS Macro Lett.* 2022, 11, 284−288 Read Online

ACCESS | Metrics & More | Article Recommendations | Supporting Information

ABSTRACT: There are long-standing debates in crystallization mechanism of polymer chains at the molecular levels: Which comes first, chain folding or lamellae formation during crystallization? In this study, we report the local chain trajectory of ^{13}C-labeled semicrystalline polymer in an extreme case of rapidly quenched glassy state as well as thermodynamically stable crystals formed via different pathways from glass and melt. Magnetically dipole interactions do not require a long-range order of molecular objects and thus enable us to trace the local chain trajectory of polymer chains even in a glassy state. To accurately characterize the local chain trajectory of polymer glass, the natural abundance effect on ^{13}C−^{13}C double-quantum (DQ) nuclear magnetic resonance (NMR) signal is re-examined using extended chain conformation. As results, it is found that glassy chains adopt the same adjacent re-entry structure (adjacent re-entry number, n = 1) with the melt- and cold-grown crystals. From these results, it is concluded that (i) folding occurs prior to crystallization and (ii) melt and cold crystallization do not induce additional folding but proceed with rearrangements of polymer chains in the existing templates.

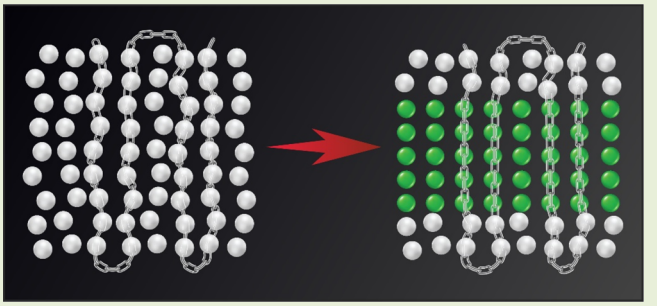

Downloaded via UNIV OF AKRON on June 28, 2022 at 16:18:22 (UTC).
See https://pubs.acs.org/sharingguidelines for options on how to legitimately share published articles.

Crystallization of long polymer chains induce structural changes from random coils in the melt to thin and folded lamellae, when the polymer melt is cooled to a certain crystallization temperature (T_c).[1−5] Flexibility and connectivity of polymers induce a chain-folding structure, which creates intramolecular packing in addition to intermolecular packing.[6] The latter commonly governs crystallization of ion, mineral, small molecule, large protein, *etc.*[7] Competition of intra- and intermolecular packing is the unique feature in polymer crystallization. Various theories and models have been proposed in polymer crystallization in the past few decades.[8−14] Among them, the well-known Lauritzen−Hoffman (LH)[8,9] theory predicts that polymer chains are dragged on the existing lamellae (secondary nucleation) and fill the layer (growth), where chain-folding structure is formed on the growth front and highly depends on T_c. Another model is the multistage model,[10] where polymer chains gradually change their own structures from disordered states to ordered ones.

In the past two decades, several important findings have been reported in both experimental[15−28] and computational works.[29−33] For example, chip DSC (cDSC) provided formations of nuclei for poly(L-lactic acid) (PLLA),[15] *isotactic*-poly(1-butene) (*i*PB1),[16] poly(ε-caprolactone),[17] *etc.*, even below the glass transition temperature, T_g. Homogeneous (primary) nucleation does not require segmental motions associated with T_g. In-situ FT-IR,[18,19] Raman,[20] and wide- (WAXS)[18,19] and small-angle X-ray scattering (SAXS)[19,21,22] measurements observed preordered structures prior to crystallization. By using ^{13}C−^{13}C DQ NMR spectroscopy,[28] it was demonstrated that adjacent re-entry structures of ^{13}C-labeled PLLA,[6] *i*PB1,[23−26] *and* *i*-polypropylene (*i*PP)[27] were invariant in a wide range of T_cs. Increasing computation power enabled one to investigate detailed molecular images in polymer crystallization.[29−33] For example, the coarse-grained (CG) poly(vinyl alcohol) (PVA) model[29−31] gave T_c independence of the adjacent re-entry structure during crystallization. These experimental[23−27] and simulation[29−31] results are not consistent with the LH theory.[8,9] However, an important question remains unsolved: *Do polymer chains fold prior to crystallization?* In other words, *which comes first: chain folding or lamellae formation?* Answering this question will provide a detailed mechanism about polymer crystallization at the molecular level.

In this work, we investigate the local chain trajectory of PLLA in thermodynamically stable crystals formed via melt and cold crystallization and an extreme limit of glassy state by using ^{13}C−^{13}C DQ NMR spectroscopy. Dipolar interaction is inversely proportional to cubic internuclear distance, r of interacting ^{13}C spins at r < 7 Å, and thus has been used to trace the local chain trajectory of ^{13}C-labeled chains diluted by nonlabeled chains (Figure 1a).[23−28] This approach does not

Received: December 16, 2021
Accepted: February 4, 2022
Published: February 8, 2022

ACS Publications © 2022 American Chemical Society

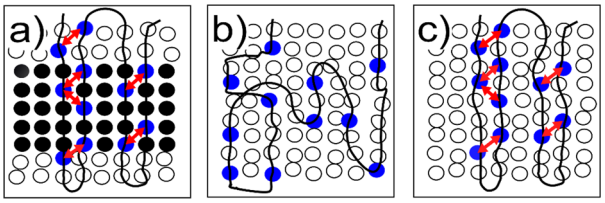

Figure 1. Schematic illustration for $^{13}C-^{13}C$ DQ NMR analysis for adjacent re-entry structure of ^{13}C-labeled chains (black lines) in (a) the crystalline regions and (b, c) the glassy state. Open and filled black and blue spheres mean amorphous and crystalline and ^{13}C-labeled monomer units, respectively. Black line and red arrows represent chain connectivity and magnetic dipole−dipole interactions, respectively.

require long-range order of molecular objects and thus can be applied to investigate local chain trajectory and packing structure in a glassy state. Two extreme cases of highly disordered and locally ordered chain trajectories were schematically depicted in parts b and c of Figure 1, respectively. By comparisons of experimental and simulated DQ buildup curves, it is demonstrated that glassy polymer chains adopt similar chain trajectories with the thermodynamically stable crystals.

^{13}C CH_3 33% labeled PLLA with weight-average molecular weight, M_w = 2.0 and 300 kg/mol, and nonlabeled PLLA with M_w = 2.3 and 248 kg/mol and nonlabeled poly(D-lactic acid) (PDLA) with M_w = 2.1 kg/mol were synthesized (see details in the Experimental Section in the Supporting Information). Their molecular weight, polydispersity, and abbreviation name are listed in Table 1.

Table 1. Weight-Average Molecular Weight, M_w, and PDI of ^{13}C 33% CH_3-Labeled and Non-Labeled PLA Used in This Work

name	M_w (kg/mol)[a]	PDI
^{13}C *h*-PLLA	300	2.26
h-PLLA	248	2.28
^{13}C *l*-PLLA	2.0	1.24
l-PLLA	2.3	1.26
l-PDLA	2.1	1.23

[a]M_w was corrected by a factor of 0.58 by using polystyrene as standard.

Figure 2a shows SAXS patten for the stereocomplex *l*-PLA crystals. The first order SAXS peak appears at q = 0.073 Å, which corresponds to a long period, l_0 of 8.6 nm in terms of $l_0 = 2\pi/q$.[34] From M_w and 3_1 helical conformation in the stereocomplex,[35,36] the chain lengths of ^{13}C *l*-PLLA, *l*-PLLA, and *l*-PDLA correspond to 7.7, 9.1, and 8.1 nm, respectively. The weight average of the chain length of 8.5 nm is close to the l_0 value. This means that the stereocomplex sample adopts an extended chain conformation. This sample is used to further calibrate the DQ signals of the ^{13}C *l*-PLLA stereocomplex.

DQ NMR could detect $^{13}C-^{13}C$ spin pair interactions within the labeled chains as well as between the labeled and nonlabeled ones. In the case of adjacent re-entry clusters, the former is dominant over the latter. However, decreasing the adjacent re-entry number, n, relatively increases the contribution from the latter to the DQ signal. This effect might overestimate n.[6,23] In particular, characterization of the n = 0 structure requires precise evaluations from natural abundance.

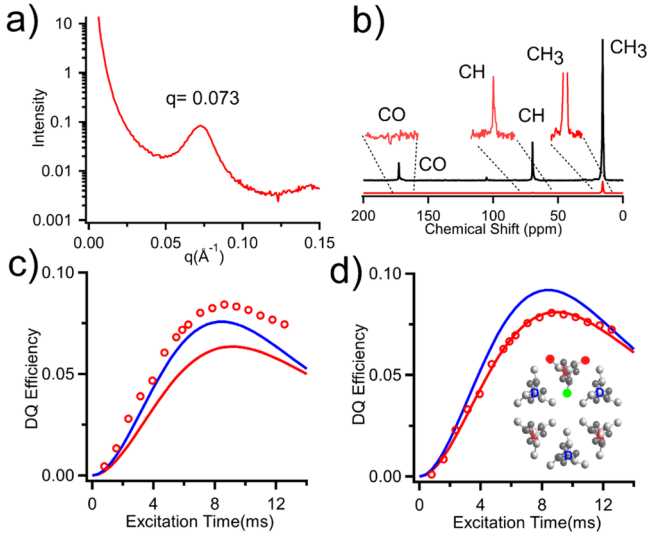

Figure 2. (a) SAXS profile for the stereocomplex reference sample. (b) ^{13}C CPMAS SQ (black) and DQ (red) NMR spectra for ^{13}C *l*-PLLA stereocomplex blend with insertion of the vertically enlarged DQ spectra by 20 times. ^{13}C DQ experimental and simulated buildup curves for ^{13}C *l*-PLLA stereocomplex blend in (c) previous and (d) current analyses. The atomic coordinates being referred to ref 37. and T_2 = 8.5 ms in the simulations. The red and blue curves representing simulation curves with n = 1 and 0, respectively in (c) the previous[23,37] and (d) the updated analyses. The inset in part d shows the packing structure for the isolated ^{13}C *l*-PLLA stem in the stereocomplex.

There are two types of natural abundance contributions. One is the CH_3 carbon, and the other is different carbons. In the previous works,[6,23] the latter was obvious in the short excitation time, τ_{ex} and was subtracted from the ^{13}C-labeled CH_3 DQ signal.[6,23] In this work, DQ signals were accumulated up to 20K times, instead of a typical 2K ones.[6] Figure 2b depicts ^{13}C CPMAS NMR spectrum (black line) for ^{13}C *l*-PLLA stereocomplex blend with *l*-PLLA and *l*-PDLA with a mixing ratio of 1:4:5, respectively. The CH_3 signal appears at 15.6 ppm, which is attributed to the stereocomplex crystals.[36,37] The DQ spectrum (red line) was obtained at τ_{ex} = 7.84 ms. The vertically enlarged DQ spectrum by 20 folds shows a small DQ signal for the CH carbon with a relative intensity of 5% to the CH_3 signal. The DQ signal from the CH carbon was subtracted from the CH_3 DQ signal. Furthermore, previous works did not consider the natural abundance effect from nonlabeled CH_3 carbons.[23,37] Here, the natural abundance effect was included in the experimental result. This procedure apparently decreases the height of DQ experimental curve compared to the previous works.[6,23,37] Figure 2c, d depicts $^{13}C-^{13}C$ DQ buildup curve (open red circles) for the ^{13}C *l*-PLLA stereocomplex blends. The maximum DQ efficiency, ξ_{max} is 8.1% at τ_{ex} = 8.62 ms. Figure 2c represents the simulation curves with n = 0 (red curve) and 1 (blue) in the previous analysis (see details in the Supporting Information).[37] The n = 1 curve (hairpin) is apparently lower than the experimental curve. The folding structure (n > 1) is not consistent with the extended chain conformation obtained by SAXS. This discrepancy is attributed to the natural abundance effect of the CH_3 carbon. The natural abundance effect was included in the simulation. The statistical interchain effect of both ^{13}C CH_3 labeled and nonlabeled chains was considered in a 10000 × 10000 stem matrix, where all

https://doi.org/10.1021/acsmacrolett.1c00789
ACS Macro Lett. 2022, 11, 284−288

probabilities from different interchain effects were generated in Monte Carlo (MC) simulation.[38] (see details in the Supporting Information). The updated simulation curves are plotted in Figure 2d. The n = 0 curve reproduces the experimental data. Under these revisions, the packing and folding structures of PLLA glass and thermodynamically stable crystals are investigated.

Figure 3a schematically illustrates experimental procedures for melt and cold crystallization as well as quenching into a glassy state used in this work (see details in the Supporting Information). T_c was set to 150 °C which is slightly higher than the reported regime I−II transition temperature of 147 °C in PLLA.[39] ^{13}C CPMAS NMR spectra and polarized optical microscope (POM) WAXS for ^{13}C h-PLLA crystal blends with h-PLLA formed via melt and cold crystallization as well as corresponding quenched ones are depicted in Figure 3b−d. In the POM images, nucleation density is limited and individual spherulites well develop with a diameter over 500 μm in melt-grown crystals whereas numerous spherulites with a limited diameter of 10−20 μm are formed in cold-grown crystals at the same T_c. The large differences in morphologies are explained in terms of formation of nucleation below T_g.[15−17] On the other hand, there is no spherulite in the quenched sample. ^{13}C CPMAS NMR spectra and WAXS patterns for the 10% ^{13}C h-PLLA blends confirm that melt- and cold-grown crystals adopt the α form[6,40] while the quenched sample adopts a glassy structure.[6,41] Interestingly, the NMR result indicates that the glassy sample gives a broad singlet CH_3 peak with full-line width at half height of ca. 200 Hz at 16.6 ppm, which are comparable to those for a kinetically favored α' crystal (180 Hz and 16.9 ppm).[41] The similarities in both the chemical shift values and line widths imply that the glassy sample adopts a similar local structure with the α' crystal. Moreover, recent fiber XRD[19] and FT-IR,[19] and Raman[42,43] analyses indicated that PLLA glass adopts similar helical conformation with that for the α (α') crystals. Due to the structural similarity between the crystal and glass, Tashiro et al. named PLLA glass as mesophase.[19] Under the assumption of the same conformation between the glass and the α crystal, the packing structure of ^{13}C h-PLLA quenched glass is investigated by using ^{13}C−^{13}C DQ NMR. The experimental DQ buildup curves for the ^{13}C h-PLLA melt-grown crystals and glass are depicted in parts a and b of Figure S6, respectively. The simulation curve was calculated by using the reported atomic coordinates of the CH_3 carbons in orthorhombic lattice (a = 10.66, b = 6.16, and c = 28.88 Å)[41] and a ^{1}H transverse relaxation time, T_2, of 9.2 ms. The chain center-to-center distance, R of the PLLA α crystals is 6.1 Å.[40] Moreover, DQ curves were simulated by changing R values to 5.9 (green curve) and 6.3 Å (blue). It is indicated that R = 6.1 ± 0.2 Å is quite consistent with the XRD result.[40] Interestingly, it is found that the PLLA glass adopts the same packing structure (R = 6.1 Å) as the α crystal. This result implies that ordering in the conformation accompanies packing with neighbors even in the glassy state.

The same strategy can be applied to the analysis for local chain trajectory in the ^{13}C h-PLLA glass and crystal blends diluted with h-PLLA. The experimental DQ buildup curves for ^{13}C h-PLLA melt-grown crystal (red open circle) and cold-grown crystal blends (green) with h-PLLA are plotted in Figure 4a. Both curves are well consistent with each other.

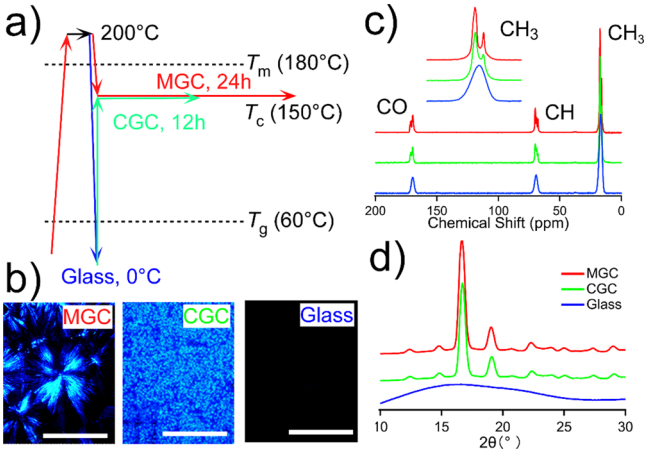

Figure 3. (a) Schematic illustrations of thermal procedures used in this work. (b) POM images, (c) ^{13}C CPMAS NMR spectra, and (d) WAXS patterns of ^{13}C h-PLLA melt-grown crystal (MGC) (red), cold-grown crystal (CGC) (green), and quenched glass (blue) blends with h-PLLA. The white scale bars represent a 500 μm scale in the POM images.

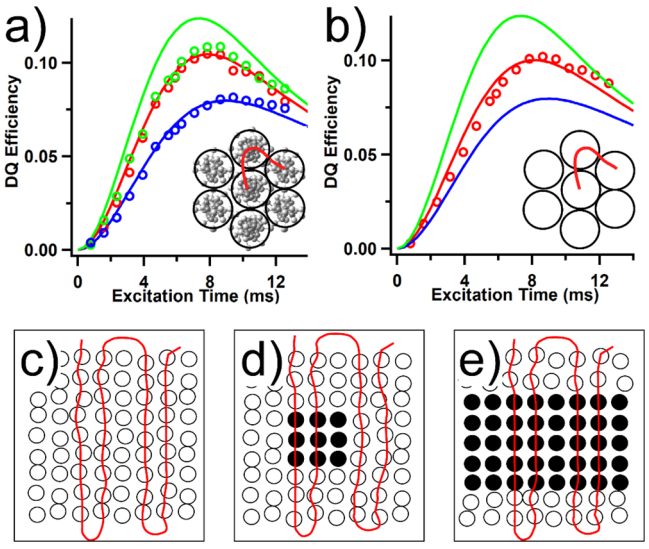

Figure 4. Experimental DQ buildup curves for (a) ^{13}C h-PLLA melt-grown (open red circles) and cold-grown crystal (green) and l-PLLA melt-grown crystal blends (blue) and (b) ^{13}C h-PLLA glass blend (open red), and simulated curves with n = 0 (blue solid), 1 (red), and 2 (green). Schematic illustration for chain trajectory with n = 1 and spatial distribution of monomer units (segments) in (c the) glassy state and (d) nucleation and (e) crystallization processes. Open and filled circles and solid red lines represent amorphous and crystalline monomer units and local chain trajectory, respectively.

Moreover, the ^{13}C l-PLLA melt-grown crystal blend expectedly shows a much smaller curve (blue open circles) than that for ^{13}C h-PLLA crystal blend. Under the assumption of R = 6.1 Å, simulated curves based on isolated chain (n = 0) and single (n = 1) and double folds (n = 2) are shown as solid blue, red, and green curves, respectively in Figure 4a. The n = 0 curve well reproduces the experimental data for ^{13}C l-PLLA melt-grown crystal blend. The experimental curves for ^{13}C h-PLLA melt- and cold-grown crystal blends are fitted with the n = 1 curve. The result of n = 1 means the same probability for intermolecular[32] and intramolecular packing.[33] This value is

https://doi.org/10.1021/acsmacrolett.1c00789
ACS Macro Lett. 2022, 11, 284−288

close to n = 1.2 for the CG-PVA model obtained in computer simulation.[30]

Figure 4b represents the experimental curve for the ^{13}C *h*-PLLA glass blend (red open circles) with the simulation curves based on the atomic coordinates for the α crystals (R = 6.1 Å). Surprisingly, it is found that the DQ curve in the glass is almost the same to those in the melt- and cold-grown crystals. Namely, glassy polymer chains adopt not random trajectory but the same hairpin structure (n = 1) (Figure 4c) with melt- and cold-grown crystals (Figure 4e). Interestingly, the folded chains form the same intramolecular packing structure of R = 6.1 Å with the α crystals. These results indicate that glassy chains adopt the same hairpin structure accompanying the tight packing with the α crystals. In nucleation and crystallization process, polymer chains rearrange their packing and conformations to form three-dimensionally ordered crystals in the existing chain templates. Such molecular events are well consistent with multistage[10,11] and solidification models.[11] The same chain-trajectory before and after crystallization might explain recently reported results in PLLA and others such as (i) homogeneous nucleation below T_g,[15−17] (ii) conformational ordering in the prestage of crystallization,[18−20,42,43] and (iii) T_c independence of adjacent re-entry structure in the melt-grown crystals.[6,23−27]

Another important aspect is formation of the fold loops in melt- and cold-grown crystals. A recent CG PVA model implied that chain folding occurs between entanglements.[29,30] The NMR results obtained in this study can be explained in terms of the mechanism provided by the MD simulation. In the case of folding prior to crystallization, the loop may not be necessarily tight. The length may be related to the late stage of crystallization. In various semicrystalline polymers, the variations in the lamellae thickness are attributed to chain mobility in the crystalline regions.[44] Thermally activated molecular dynamics increases the thickness of lamellae and thus the process may push the crystal−amorphous boundary up to the vicinity of the fold surface (Figure 4e) and may resultantly make tight loops at the fold surface. Otherwise, polymer chains would adopt loose and long loops in the melt- and cold-grown crystals.

In summary, chain-folding and local packing structures of PLLA in a quenched glassy state as well as thermodynamically stable α crystals were investigated by $^{13}C-^{13}C$ DQ NMR spectroscopy. It was found that glassy PLLA adopts the similar packing structure with that for the crystals. Moreover, it was demonstrated that glassy PLLA chains adopt the same one-fold (n = 1) and intramolecular packing (R = 6.1 Å) structures with the thermodynamically stable crystals formed via melt and glassy states. From the results, it is concluded that polymer chains fold prior to crystallization, and nucleation and crystallization proceed via rearrangements of polymer chains in the existing chain templates.

■ ASSOCIATED CONTENT

Supporting Information

The Supporting Information is available free of charge at https://pubs.acs.org/doi/10.1021/acsmacrolett.1c00789.

Synthesis protocol, experimental conditions, Monte Carlo simulation results, and packing analysis by DQ NMR (PDF)

■ AUTHOR INFORMATION

Corresponding Author

Toshikazu Miyoshi − *School of Polymer Science and Polymer Engineering, The University of Akron, Akron, Ohio 44325-3909, United States;* orcid.org/0000-0001-8344-9687; Email: miyoshi@uakron.edu

Authors

Fan Jin − *School of Polymer Science and Polymer Engineering, The University of Akron, Akron, Ohio 44325-3909, United States*

Shichen Yuan − *School of Polymer Science and Polymer Engineering, The University of Akron, Akron, Ohio 44325-3909, United States*

Shijun Wang − *School of Polymer Science and Polymer Engineering, The University of Akron, Akron, Ohio 44325-3909, United States*

Yi Zhang − *School of Polymer Science and Polymer Engineering, The University of Akron, Akron, Ohio 44325-3909, United States*

Ying Zheng − *School of Polymer Science and Polymer Engineering, The University of Akron, Akron, Ohio 44325-3909, United States; State Key Laboratory of Chemical Engineering, College of Chemical and Biological Engineering, Zhejiang University, Hangzhou 310027, China; Institute of Zhejiang University-Quzhou, Quzhou 324000, China;* orcid.org/0000-0002-2379-6342

You-lee Hong − *School of Polymer Science and Polymer Engineering, The University of Akron, Akron, Ohio 44325-3909, United States*

Complete contact information is available at: https://pubs.acs.org/10.1021/acsmacrolett.1c00789

Author Contributions

#F.J. and S.Y. equally contributed to the first authorship. F.J. and S.W. synthesized samples. F.J., S.Y., S.W., Y.H., and T.M. conceived and designed experiments. F.J. and S.Y. conducted NMR, WAXS, and POM experiments and simulations. Y.Z. conducted SAXS experiments. The manuscript was written through contributions of all authors. All authors have given approval to the final version of the manuscript.

Notes

The authors declare no competing financial interest.

■ ACKNOWLEDGMENTS

This work was financially supported by NSF DMR Polymers 1708999 and 2004393.

■ REFERENCES

(1) Corradini, P.; Auriemma, F.; De Rosa, C. Crystals and Crystallinity in Polymeric Materials. *Acc. Chem. Res.* **2006**, *39*, 314−323.

(2) Strobl, G. Crystallization and melting of bulk polymers: New observations, conclusions and a thermodynamic scheme. *Prog. Polym. Sci.* **2006**, *31*, 398−442.

(3) Cheng, S. Z. D. *Phase Transitions in Polymers*; Elsevier: 2008.

(4) Lotz, B.; Miyoshi, T.; Cheng, S. Z. D. 50th Anniversary Perspective: Polymer Crystals and Crystallization: Personal Journeys in a Challenging Research Field. *Macromolecules* **2017**, *50*, 5995−6025.

(5) Tang, X.; Chen, W.; Li, L. The Tough Journey of Polymer Crystallization: Battling with Chain Flexibility and Connectivity. *Macromolecules* **2019**, *52*, 3575−3591.

(6) Wang, S.; Yuan, S.; Wang, K.; Chen, W.; Yamada, K.; Barkley, D.; Miyoshi, T.; et al. Intramolecular and Intermolecular Packing in Polymer Crystallization. *Macromolecules* **2019**, *52*, 4739−4748.
(7) De Yoreo, J. J.; Gilbert, P. U. P. A.; Sommerdijk, N. A. J. M.; Penn, R. L.; Whitelam, S.; Joester, D.; Zhang, H.; Rimer, J. D. L; Navrotsky, A.; Banfield, J. F.; Wallace, A. F.; Michel, F. M.; Meldrum, F.; Cölfen, H.; Dove, P. M. Crystallization by particle attachment in synthetic, biogenic, and geologic environments. *Science* **2015**, *349*, No. aaa6760.
(8) Lauritzen, J. I.; Hoffman, J. D. Theory of Formation of Polymer Crystals with Folded Chains in Dilute Solution. *J. Res. Natl. Bur. Stand., Sect. A* **1960**, *64A*, 73.
(9) Hoffman, J. D.; Miller, R. L. Kinetic of Crystallization from the Melt and Chain Folding in Polyethylene Fractions Revisited: Theory and Experiment. *Polymer* **1997**, *38*, 3151−3212.
(10) Strobl, G. From the melt via mesomorphic and granular crystalline layers to lamellar crystallites: A major route followed in polymer crystallization? *Eur. Phys. J. E* **2000**, *3*, 165−183.
(11) Fischer, E. W. Studies of structure and dynamics of solid polymers by elastic and inelastic neutron scattering. *Pure Appl. Chem.* **1978**, *50*, 1319−1341.
(12) Sadler, D. M. New explanation for chain folding in polymers. *Nature* **1987**, *326*, 174−177.
(13) Liu, C.; Muthukumar, M. Langevin Dynamics Simulations of Early-Stage Polymer Nucleation and Crystallization. *J. Chem. Phys.* **1998**, *109*, 2536−2542.
(14) Allegra, G.; Meille, S. V. Pre-crystalline, high-entropy aggregates: A role in polymer crystallization? In *Interphases and Mesophases in Polymer Crystallization III*; Springer: 2005; pp 87−135.
(15) Androsch, R.; Di Lorenzo, M. L. Crystal Nucleation in Glassy Poly(L-lactic acid). *Macromolecules* **2013**, *46*, 6048−6056.
(16) Stolte, I.; Androsch, R.; Di Lorenzo, M. L.; Schick, C. Effect of Aging the Glass of Isotactic Polybutene-1 on Form II Nucleation and Cold Crystallization. *J. Phys. Chem. B* **2013**, *117*, 15196−15203.
(17) Zhuravlev, E.; Schmelzer, J. W. P.; Wunderlich, B.; Schick, C. Kinetics of nucleation and crystallization in poly(ϵ-caprolactone) (PCL). *Polymer* **2011**, *52*, 1983−1997.
(18) Sasaki, S.; Tashiro, K.; Kobayashi, M.; Izumi, Y.; Kobayashi, K. Microscopically viewed structural change of PE during the isothermal crystallization from the melt: II. Conformational ordering and lamellar formation mechanism derived from the coupled interpretation of time-resolved SAXS and FTIR data. *Polymer* **1999**, *40*, 7125−7135.
(19) Wasanasuk, K.; Tashiro, K. Structural regulation in the Crystallization Process from the Glass or Melt of Poly(L-Lactic Acid) Viewed from the Temperature-Dependent and Time-Resolved Measurements of FTIR and Wide-Angle/Small-Angle X-ray Scatterings. *Macromolecules* **2011**, *44*, 9650−9660.
(20) Migler, K. B.; Kotula, A. P.; Hight Walker, A. R. Trans-Rich Structures in Early Stage Crystallization of Polyethylene. *Macromolecules* **2015**, *48*, 4555−4561.
(21) Konishi, T.; Okamoto, D.; Tadokoro, D.; Kawahara, Y.; Fukao, K.; Miyamoto, Y. Origin of SAXS Intensity in the low-q region during the early stage of polymer crystallization from both the melt and glassy state. *Phys. Rev. Materials* **2018**, *2*, 105602.
(22) Li, X.; Ding, J.; Chen, P.; Zheng, K.; Zhang, X.; Tian, X. Detection and characterization of folded chain clusters in the structured melt of isotactic polypropylene. *IUCrJ.* **2021**, *8*, 595−607.
(23) Hong, Y. L.; Miyoshi, T. Chain-Folding Structure of a Semicrystalline Polymer in Bulk Crystals Determined by ^{13}C-^{13}C Double Quantum NMR. *ACS Macro Lett.* **2013**, *2*, 501−505.
(24) Hong, Y. L.; Koga, T.; Miyoshi, T. Chain Trajectory and Crystallization Mechanism of a Semicrystalline Polymer in Melt- and Solution-Grown Crystals As Studied Using ^{13}C-^{13}C Double-Quantum NMR. *Macromolecules* **2015**, *48*, 3282−3293.
(25) Hong, Y. L.; Yuan, S.; Li, Z.; Ke, Y.; Nozaki, K.; Miyoshi, T. Three-Dimensional Conformation of Folded Polymers in Single Crystals. *Phys. Rev. Lett.* **2015**, *115*, 168301.
(26) Hong, Y. L.; Chen, W.; Yuan, S.; Kang, J.; Miyoshi, T. Chain Trajectory of Semicrystalline Polymers As Revealed by Solid-State NMR Spectroscopy. *ACS Macro Lett.* **2016**, *5*, 355−358.
(27) Yuan, S.; Li, Z.; Hong, Y. L.; Ke, Y.; Kang, J.; Kamimura, A.; Otsubo, A.; Miyoshi, T. Folding of Polymer Chains in the Early Stage of Crystallization. *ACS Macro Lett.* **2015**, *4*, 1382−1385.
(28) Hohwy, M.; Jakobsen, H. J.; Edén, M.; Levitt, M. H.; Nielsen, N. C. Broadband Dipolar Recoupling in the Nuclear Magnetic Resonance of Rotating Solids: A Compensated C7 Pulse Sequence. *J. Chem. Phys.* **1998**, *108*, 2686−2694.
(29) Luo, C.; Sommer, J. U. Growth Pathway and Precursor States in Single Lamellar Crystallization: MD Simulations. *Macromolecules* **2011**, *44*, 1523−1529.
(30) Luo, C.; Sommer, J. U. Role of thermal history and entanglement related thickness selection in polymer crystallization. *ACS Macro Lett.* **2016**, *5*, 30−34.
(31) Luo, C.; Kröger, M.; Sommer, J.-U. Entanglements and crystallization of concentrated polymer solutions: molecular dynamics simulations. *Macromolecules* **2016**, *49*, 9017−9025.
(32) Hu, W.; Cai, T. Regime Transitions of Polymer Crystal Growth Rates: Molecular Simulations and Interpretation beyond Lauritzen-Hoffman Model. *Macromolecules* **2008**, *41*, 2049−2061.
(33) Yi, P. C.; Locker, R.; Rutledge, G. C. Molecular Dynamics Simulation of Homogeneous Crystal Nucleation in Polyethylene. *Macromolecules* **2013**, *46*, 4723−4733.
(34) Strobl, G. *The Physics of Polymers*, 3rd ed.; Springer-Verlag Berlin Heidelberg: 2007.
(35) Cartier, L.; Okihara, T.; Lotz, B. Triangular Polymer Single Crystals: Stereocomplexes Twins and Frustrated Structure. *Macromolecules* **1997**, *30*, 6313−6322.
(36) Zhou, W.; Wang, K.; Wang, S.; Yuan, S.; Chen, W.; Konishi, T.; Miyoshi, T. Stoichiometry and Packing Structure of Poly(Lactic Acid) Stereocomplex as Revealed by Solid state NMR and ^{13}C Isotope Labeling. *ACS Macro Lett.* **2018**, *7*, 667−671.
(37) Chen, W.; Wang, S.; Zhang, W.; Ke, Y.; Hong, Y.-L.; Miyoshi, T. Molecular Structural Basis for Stereocomplex Formation of Poly(Lactide)s in Dilute Solution. *ACS Macro Lett.* **2015**, *4*, 1264−1267.
(38) Frenkel, D. Introduction to Monte Carlo Methods. *NIC Series* **2004**, *23*, 29−60.
(39) Miyata, T.; Masuko, T. Crystallization behavior of poly(L-lactide). *Polymer* **1998**, *39*, 5515−5521.
(40) Sasaki, S.; Asakura, T. Helix Distortion and Crystal Structure of the α-Form of Poly (L -Lactide). *Macromolecules* **2003**, *36*, 8385−8390.
(41) Chen, W.; Zhou, W.; Makita, Y.; Wang, S.; Yuan, S.; Konishi, T.; Miyoshi, T. Characterization of the Slow Molecular Dynamics of Poly(l-Lactic Acid) in α and α' Phases, in a Glassy State, and in a Complex with Poly(D-Lactic Acid) by Solid-State NMR. *Macromol. Chem. Phys.* **2018**, *219*, 1700451.
(42) Yang, X.; Kang, S.; Yang, Y.; Aou, K.; Hsu, S. L. Raman spectroscopic study of conformational changes in the amorphous phase of poly(lactic acid) during deformation. *Polymer* **2004**, *45*, 4241−4248.
(43) Yang, X.; Kang, S.; Hsu, S. L.; Stidham, H. D.; Smith, P. B.; Leugers, A. A Spectroscopic Analysis for Chain Flexibility of Poly(lactic acid). *Macromolecules* **2001**, *34*, 5037−5041.
(44) Kafle, N.; Makita, Y.; Zheng, Y.; Kurosu, H.; Pan, P.; Nakama, Y.; Hayano, S.; Miyoshi, T.; et al. Roles of Conformational Flexibility for the Crystallization of Stereo-irregular Polymer. *Macromolecules* **2021**, *54*, 5705−5718.

https://doi.org/10.1021/acsmacrolett.1c00789
ACS Macro Lett. 2022, 11, 284−288